

Charge order at magnetite $\text{Fe}_3\text{O}_4(001)$: surface and Verwey phase transitions

I. Bernal-Villamil, S. Gallego*

*Instituto de Ciencia de Materiales de Madrid, Consejo Superior
de Investigaciones Científicas, Cantoblanco, 28049 Madrid, Spain*

(Dated: July 1, 2018)

At ambient conditions, the $\text{Fe}_3\text{O}_4(001)$ surface shows a $(\sqrt{2} \times \sqrt{2})R45^\circ$ reconstruction that has been proposed as the surface analog of the bulk phase below the Verwey transition temperature, T_V . The reconstruction disappears at a high temperature, T_S , through a second order transition. We calculate the temperature evolution of the surface electronic structure based on a reduced bulk unit cell of $P2/m$ symmetry that contains the main features of the bulk charge distribution. We demonstrate that the insulating surface gap arises from the large demand of charge of the surface O, at difference with that of the bulk. Furthermore, it is coupled to a significant restructuration that inhibits the formation of trimerons at the surface. An alternative bipolaronic charge distribution emerges below T_S , introducing a competition between surface and bulk charge orders below T_V .

PACS numbers: 73.20.At, 68.47.-b, 68.35.Rh, 68.35.B-

I. INTRODUCTION

Magnetite (Fe_3O_4) is the oldest known magnet and a fascinating material both for understanding the fundamental physics that emerge from electronic correlations, and for novel technologies related to oxide electronics¹⁻³. At ambient conditions, it crystallizes in the inverse spinel structure with cubic $Fd\bar{3}m$ symmetry. The O atoms form a fcc lattice, with Fe_A atoms in tetrahedral sites acting with a nominal +3 valence, and Fe_B cations with +2.5 valence in octahedral positions. The Fe_A and Fe_B sublattices are antiferromagnetically coupled, and the minority spin t_{2g} states of the Fe_B atoms cross the Fermi level, leading to a half-metallic ferrimagnet with high magnetic moment, 4 μ_B per formula unit (f.u.).

At a critical temperature $T_V \sim 120$ K, magnetite undergoes the first-order Verwey transition (VT), that manifests in a structural modification to a monoclinic symmetry accompanied by a drop of the conductivity of 2-3 orders of magnitude⁴. The decrease of the conductivity is due to a freezing of the electron hopping between different octahedral Fe sites, causing a charge disproportionation that results in two types of Fe_B atoms acting with a slightly enhanced (Fe^{3+}) or reduced (Fe^{2+}) valence. The distribution of the different Fe_B atoms at the unit cell configures the charge order (CO), intimately linked to the orbital order^{5,6}, and determines the full monoclinic Cc symmetry⁷⁻¹¹. Decades of efforts have been devoted to the understanding of the VT^{12,13}, and yet some puzzling fundamental aspects remain unanswered, such as the structural or electronic origin of the transition, or the extent of the short range order above T_V . The present consensus is that the phase transition is governed by electron-phonon couplings in the presence of strong electronic correlations¹⁴. A local perturbation of the extended CO has been recently identified in the form of trimerons: linear chains of three adjacent Fe_B cations dominantly formed by a central Fe^{2+} and two Fe^{3+} , with a significant reduction of the interatomic Fe-Fe distances and a polaronic distribution of shared

charge¹¹. Trimerons reveal as the essential short-range unit in the electronic phase transitions of magnetite¹⁵. Furthermore, laser pump-probe experiments have created a non-equilibrium version of the VT by introducing holes in the trimeron lattice¹⁶. This invokes the possibility to obtain analogs of the VT under sizes much lower than those required by a full Cc cell, and in fact, as a first result of this work, we will demonstrate the ability of trimerons to emerge in a reduced unit cell of $P2/m$ symmetry.

One of the handicaps for the exploitation of the VT in novel technologies is the low value of T_V , well below room temperature (RT). The measurement at the $\text{Fe}_3\text{O}_4(001)$ surface of an insulating gap at RT¹⁷ and the further prediction that its existence was accompanied by a subsurface CO similar to the bulk one¹⁸, caused thus great excitement. $\text{Fe}_3\text{O}_4(001)$ presents a $(\sqrt{2} \times \sqrt{2})R45^\circ$ reconstruction which corresponds to a bulk truncation at an Fe_B -O plane¹⁹⁻²¹. Its origin has been assigned to a Jahn-Teller distortion causing a wavelike displacement of the Fe_B surface atoms along $\langle 110 \rangle$ directions^{22,23}. Seemingly this RT reconstruction is not significantly altered across the VT^{23,24}. However, the evolution in depth of the subsurface CO has not been investigated, setting forth interrogants about the formation of surface trimerons and the relation between the surface and bulk COs below T_V . A recent study proves that the bulk low temperature phase (LTP) manifests at the surface in distinct structural features than the reconstruction²⁴. Furthermore, the $(\sqrt{2} \times \sqrt{2})R45^\circ$ symmetry is lost in favor of a (1×1) structure at a temperature $T_S \sim 720$ K through a second-order transition involving loss of long-range CO²⁵. These results suggest the existence of fundamental differences between the surface and bulk insulating phases.

In this work we provide firm proof of this fact, calculating the evolution with temperature of the electronic structure of the $\text{Fe}_3\text{O}_4(001)$ surface. Our results evidence that the surface insulating state originates from the combination of large O electron affinity and loss of O

bonds, and remains unaltered across the bulk and surface transitions. This has an impact for the disappearance of trimers close to the surface, replaced by bipolaronic structures below T_S . As a consequence, a competition between the local bulk and surface COs emerges below T_V , that manifests in modulations of the surface CO arising both from bulk trimers and from the surface reconstruction.

II. THEORETICAL METHOD

We have performed first principles calculations of both bulk magnetite and its (001) termination, based on the density functional theory including correlation effects. We employ a plane wave basis set²⁶ and the projector augmented waves (PAW) method to describe the core electrons²⁷, with an energy cutoff of 400 eV and a Monkhorst-Pack sampling of the Brillouin zone (BZ) of $(7 \times 7 \times 5)$ for the bulk and up to $(6 \times 6 \times 2)$ for the surface slabs, that guarantee convergence in the total energy better than 0.1 meV/f.u. We use the exchange-correlation functional parametrization of Perdew-Burke-Erzenhof (PBE), adding an effective on-site Coulomb repulsion term $U=4$ eV²⁸. This choice of U is based on the recovery of an equilibrium value of the cubic lattice parameter $a = 8.4$ Å in excellent agreement with experiments, and the adequate description of the Verwey transition in terms of charge disproportionation ($0.27 e$) and electronic band gap (0.2 eV) when reducing the symmetry from the cubic $Fd\bar{3}m$.

Our description of bulk magnetite is based on a $P2_1/m$ unit cell formed by 28 atoms. We have determined the equilibrium structures above and below T_V starting from the ideal cubic lattice and allowing relaxation of the lattice vectors and atomic positions, with no symmetry constraints for the low temperature phase (LTP). Even at the high temperature phase (HTP) there exists a noticeable distortion of the O sublattice, that introduces a slight tetragonal deformation of the unit cell with a small reduction of the total volume of 3 Å^3 . At the LTP, relaxation of the lattice vectors leads to an orthorhombic symmetry, but again the distortion of the unit cell is small, with a similar reduction of the total volume.

To model the $\text{Fe}_3\text{O}_4(001)$ surface, we have used slabs of different thicknesses, containing from 8 to 16 atomic planes, supported on a Au substrate and including a vacuum region of at least 12 Å that avoids interaction between opposite slab surfaces. The choice of the substrate has been performed to minimize interface effects and to confine them to the interface layer. In all cases we have employed $(\sqrt{2} \times \sqrt{2})R45^\circ$ two-dimensional unit cells, starting our calculations either from the (1×1) termination or from the Jahn-Teller induced wavelike pattern, and allowing to relax the atomic positions of the 3 outermost surface layers until the forces on all atoms are below 0.01 eV/Å. We have done this for slabs constructed both from the HTP and the LTP bulk structures. The slabs

of 12 planes provide the minimum thickness to recover the bulk structure at the inner layers below T_V including the distribution of trimers, and all the results presented here correspond to this configuration. We have also modelled thicker unsupported symmetric slabs of 16 planes to check the independence of our conclusions on the slab configuration, particularly concerning the penetration of surface effects.

III. BULK Fe_3O_4

Figure 1 and Table I summarize our results for the density of states (DOS), the Bader charges (Q_B) and the interatomic distances at both the HTP and the LTP of bulk magnetite. The energy barrier between both phases is 170 meV/f.u. The higher symmetry of the HTP reflects in the existence of only one type of O and Fe_B sites with a bond length of 2.06 Å, and in the uniform value of the $\text{Fe}_B\text{-Fe}_B$ interatomic distance ($d^{FF} = 2.96 \text{ Å}$).

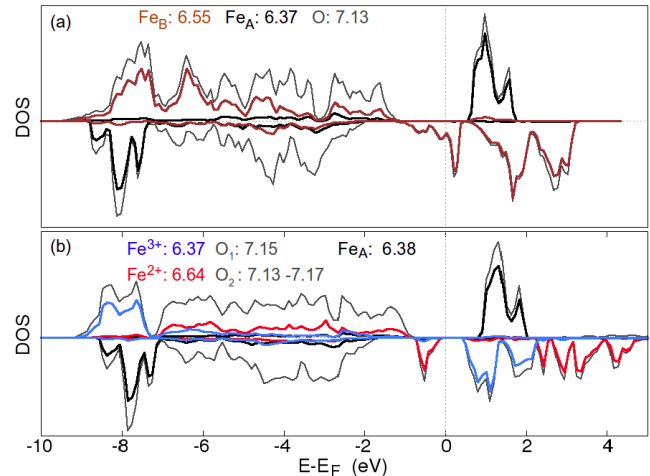


FIG. 1. (Color online) Total DOS of bulk Fe_3O_4 at the (a) HTP and (b) LTP of bulk magnetite, showing the projections on the Fe_A (thick black) and inequivalent Fe_B (red/blue) sites. Positive (negative) DOS values correspond to majority (minority) spin projections.

Below T_V , while Fe_A remains essentially unaffected by the transition, a charge disproportionation of $0.27 e$ appears in the Fe_B sublattice, opening a band gap of 0.2 eV. Within our reduced $P2_1/m$ cell, the Fe^{2+} and Fe^{3+} ions alternate along the $[001]$ direction, as evidenced in figure 2. Different values of the d^{FF} can be found depending on the Fe valence. This is accompanied by a noticeable dispersion of the $\text{Fe}_B\text{-O}$ bond lengths, with larger average values for Fe^{2+} (2.08 Å) than for Fe^{3+} (2.03 Å). The result is a non-uniform distribution of charge and magnetic moments that leads to slightly different O atoms at the Fe^{3+} (O_1) and Fe^{2+} (O_2) planes, as reflected in the dispersion of the Q_B values. However, the same net

magnetization of $4 \mu_B/\text{f.u.}$ is obtained above and below T_V .

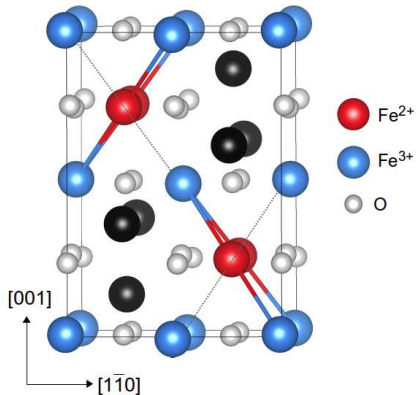


FIG. 2. Distribution of trimerons at the $P2/m$ unit cell of the LTP of bulk Fe_3O_4 .

TABLE I. Mean Fe-O bond-lengths ($d(\text{Fe-O})$) and values of the interatomic distances between first Fe_B neighbors (d^{FF}) at the HTP and LTP of bulk Fe_3O_4 . Units are Å.

$d(\text{Fe-O})$	$\text{Fe}^{2+}\text{-O}$	$\text{Fe}^{3+}\text{-O}$	$\text{Fe}_A\text{-O}$
HTP	2.06	—	1.89
LTP	2.03	2.08	1.89
d^{FF}	$\text{Fe}^{2+}\text{-Fe}^{2+}$	$\text{Fe}^{2+}\text{-Fe}^{3+}$	$\text{Fe}^{3+}\text{-Fe}^{3+}$
HTP	2.96	—	—
LTP	2.95	2.89/3.03	2.95

The inhomogeneities in the d^{FF} at the LTP have important consequences for the emergence of trimerons. Regarding figure 2, every Fe^{2+} is surrounded by 4 Fe^{3+} placed at the adjacent upper and lower (001) layers. Two of them are at 2.89Å (solid colored lines) and the other two are at 3.03Å (dotted lines), while the interatomic distance between coplanar Fe_B atoms is 2.95Å , as shown in table I. This defines linear $\text{Fe}^{3+}\text{-Fe}^{2+}\text{-Fe}^{3+}$ chains of shortened lengths, with a charge accumulation over $0.027 e/\text{Å}^3$ at the middle of each $\text{Fe}^{3+}\text{-Fe}^{2+}$ segment, in analogy with the experimental features assigned to trimerons¹¹. The orbital character of the electronic states confirms the polaronic charge distribution, with the occupied $\text{Fe}^{2+} t_{2g}$ minority spin states lying along the central axis of the chain and inducing a small contribution of the same orbital character at the closer Fe^{3+} .

Trimerons are uniquely characterized by the coexistence of all these features –short d^{FF} ($< 2.93\text{Å}$), enhanced charge accumulation ($> 0.027 e/\text{Å}^3$) and orbital directionality–, as confirmed by exploring alternative solutions without CO along the (001) direction where trimerons do not form. Moreover, the existence of

these solutions points to the complex link between the long- and short-range COs¹⁵. We have observed that, already under a cubic lattice, the reduced $P2/m$ unit cell is enough for the Verwey metal-insulator transition to emerge, merely by relaxing the symmetry constraints of the HTP in the presence of electronic correlations ($U > 2\text{eV}$)⁵. The additional full relaxation of the lattice vectors and atomic positions introduces a slight orthorhombic distortion at the LTP, and is accompanied by the formation of the local trimeron structures. This links the metal-insulator transition to the extended CO, and separates it from the short-range correlations, in good agreement with recent evidence¹⁵. Though the intricate relation between the different COs can only be ultimately integrated under the full Cc symmetry, the results presented in this section prove that our reduced unit cell contains the main features of the charge distribution at the LTP: a dominant CO along the [001] axis²⁹, and the existence of trimerons as short-range features that are distinct to the low temperature CO but intimately connected to it. This supports the use of the $P2/m$ cell as a basis to explore the surface properties below T_V .

IV. THE $\text{Fe}_3\text{O}_4(001)$ SURFACE ABOVE T_V

We will first focus on the unreconstructed surface of the HTP above T_S . A sketch of the structure corresponding to our ground state is depicted in figure 3, where layers are numbered from the surface (L1) towards the bulk. As each surface O atom has lost one donor neighbor, they reduce the bond lengths to the remaining Fe_B cations to $\sim 1.97\text{Å}$ in order to recover the bulk-like charge. This leads to a significant rearrangement of the atomic positions, where the compression of the first interlayer distance ($d_{12} = 0.78\text{Å}$, to be compared to the bulk value 1.04Å) is followed by the expansion of the subsequent interlayer spacings ($d_{23} = 1.17\text{Å}$, $d_{34} = 1.07\text{Å}$). As indicated in figure 3, at L1 there are two types of O sites, either bonded to a subsurface Fe_B (O_B) or to Fe_A (O_A). In order to avoid the excessive shortening of the O-Fe_A distance, the O_A atoms move outwards, inducing at L1 a large corrugation of 0.11Å and a slight in-plane wave-like distortion of the O rows. The asymmetry persists at L3, where the O corrugation attenuates to 0.04Å . While Fe_A remains essentially unaffected by the large distortion of the O sublattice, the opposite occurs for the Fe_B at the two outermost layers, L1 and L3. Each Fe_B along the surface [110] and subsurface $[1\bar{1}0]$ rows approaches one of their adjacent Fe neighbors at the cost of farthening from the opposite. As shown in figure 3(b), the movement is more pronounced at the subsurface.

The result of this restructuration in the electronic properties can be seen in figure 4, that provides the atomic-resolved DOS and the corresponding Q_B at the outermost $\text{Fe}_B\text{-O}$ planes, where all surface effects are contained. Although the O charges show significant dispersion, the differences are not apparent in the DOS, and

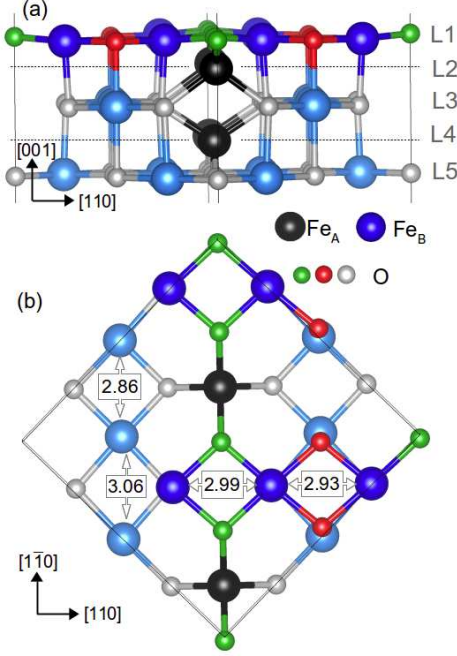


FIG. 3. (Color online) (a) Top and (b) side views of the $\text{Fe}_3\text{O}_4(001)$ surface above T_S . Panel (b) only shows the 3 outermost planes, indicating the different in-plane $\text{Fe}_B\text{-Fe}_B$ distances in Å. Also, for clarity, the leftmost surface row of O atoms is not depicted.

their Q_B are close to bulk values throughout the structure. The Fe_B atoms at L1 behave as Fe^{3+} , opening an insulating gap. However, the emergence of the gap is not accompanied by any charge disproportionation at the Fe_B sublattice. A gradual recovery of bulk-like behavior starts at L3, and is almost restored at L5. As our slabs are not completely free from confinement effects, we cannot discard that it could be restored even at L3, as inferred from STM observations of the structure of antiphase boundaries (APB)^{25,30}. It is also important to remark that although uncompensated and slightly enhanced magnetic moments emerge at the surface plane ($4.16\mu_B$ for Fe, $0.4\mu_B$ for O), the antiferromagnetic coupling between the Fe_A and Fe_B sublattices remains unaltered. This preserves the bulk-like high magnetic moment of Fe_3O_4 also at the high temperature surface, validating it as a promising material for spintronics applications.

When the temperature is lowered below T_S , the $(\sqrt{2} \times \sqrt{2})R45^\circ$ reconstruction sets in. This surface has already been studied in detail, but there are yet controversies about the origin of the reconstruction and its dependence on electronic correlations^{18,22}. Our results indicate that all effects described for the unreconstructed surface are still present below T_S , with only minor modifications of d_{23} and d_{34} of less than 0.04 Å, and slightly more asymmetric Fe-O coordination units. Figure 5 shows a sketch of the structure and figure 6 the corresponding DOS and

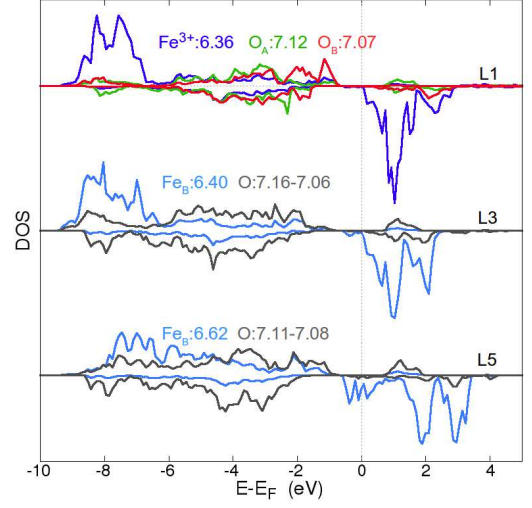


FIG. 4. (Color online) Spin-resolved DOS of all inequivalent atoms (blue for Fe, red/green for surface O) at the outermost $\text{Fe}_B\text{-O}$ planes of figure 3, providing the corresponding Q_B .

Q_B at the 3 outermost $\text{Fe}_B\text{-O}$ planes. The most relevant feature introduced by the reconstruction is the emergence of a charge disproportionation of $\sim 0.10e$ between Fe sites at L3, that defines a CO pattern within the (001) plane reducing the dispersion of O charges. This subsurface CO was already proposed on the basis of purely electronic effects¹⁸. However, we obtain that the atomic wavelike displacement at the surface Fe rows lowers the energy by 28 meV/f.u. with respect to the (1×1) surface also in the presence of electronic correlations. Reminiscence of this CO persists at L5, though half-metallicity is recovered. In fact, we cannot discard some penetration of the surface effects at deeper layers in real samples, where the existence of defects or APB may contribute to alterations of the CO, as the energy barrier between different charge distributions is of only a few meV³⁰.

From these results it is clear that the surface transition arises from the interplay between CO and electron-lattice couplings, as already proposed on the basis of thermodynamic models²⁵. But although an insulating and charge-ordered state exists below T_S , the surface introduces significant differences with the bulk LTP. At L3, the Fe charge and DOS width are influenced by the demand of charge from surface O, and show reduced values with respect to the bulk Fe^{3+} and Fe^{2+} . More important, as we will prove now, neither the surface structure nor the orbital character of the surface t_{2g} states support the definition of trimers.

Regarding figure 5, the wavelike Fe_B surface displacements define narrow and wide regions occupied respectively by Fe^{2+} and Fe^{3+} . As a result, along each subsurface $[1\bar{1}0]$ row, pairs of Fe^{2+} and Fe^{3+} alternate, inhibiting the formation of linear $\text{Fe}^{3+}\text{-Fe}^{2+}\text{-Fe}^{3+}$ chains within the (001) plane. Eventhough the longitudinal

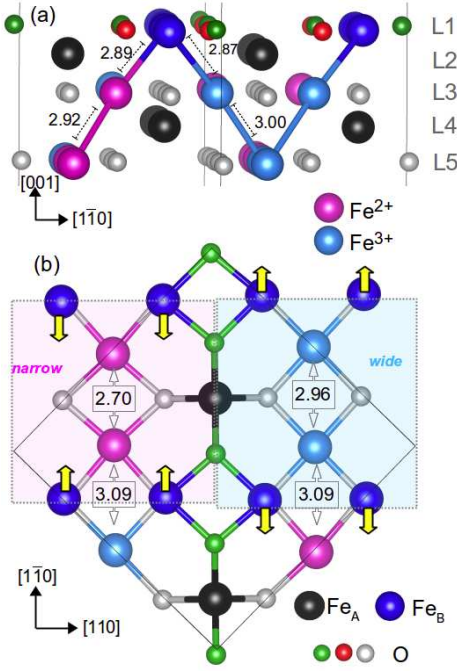


FIG. 5. (Color online) Same as figure 3 for the HTP below T_S . Values of the $\text{Fe}_B\text{-Fe}_B$ distances in Å are provided (a) between planes and (b) along the surface and subsurface Fe_B rows. Arrows in (b) are a guide to indicate the wavelike displacements of surface Fe, and only the central row of surface O atoms is depicted for clarity.

movement of the surface Fe_B along (110) rows (not shown in the figure) is similar to that above T_S , at the subsurface the displacement of Fe^{3+} is suppressed, originating shortened $d^{FF}=2.70$ Å between $\text{Fe}^{2+}\text{-Fe}^{2+}$ and large $d^{FF}=3.09$ Å between $\text{Fe}^{3+}\text{-Fe}^{2+}$. This leads to in-plane charge sharing between Fe^{2+} sites, forming a kind of localized bipolarons^{18,20} with a large charge accumulation of $0.035 e/\text{Å}^3$, but opposes to the structure of bulk trimers. This tendency persists with respect to the adjacent planes: as shown in figure 5(a), the d^{FF} to the Fe_B neighbors at L1 is similar for Fe^{3+} and Fe^{2+} , and much larger than 2.70 Å. Similarly, the Fe_B closer to subsurface Fe^{3+} (Fe^{2+}) at L5 are those of Fe^{3+} (Fe^{2+}) type, and are also farther than 2.70 Å. In conclusion, neither the interatomic distances nor the charge distribution arising from the surface reconstruction support the formation of bulk-like trimers.

V. THE $\text{Fe}_3\text{O}_4(001)$ SURFACE BELOW T_V

The different nature of the low temperature surface and bulk phases discards that the $(\sqrt{2} \times \sqrt{2})R45^\circ$ reconstruction acts as the first stage for the development of the VT. However, it suggests the possibility of a competition between surface and bulk COs below T_V . In order to explore this, we have modelled the $\text{Fe}_3\text{O}_4(001)$

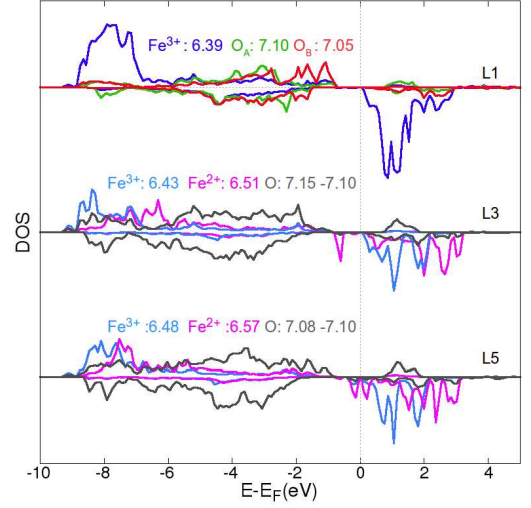


FIG. 6. (Color online) Same as figure 4 for the structure in figure 5.

surface of the LTP departing from our $P2/m$ bulk unit cell. Although this cell contains limited information of the actual long-range CO, we will show that yet important insights about the mutual influence of the bulk and surface short-range correlations become evident.

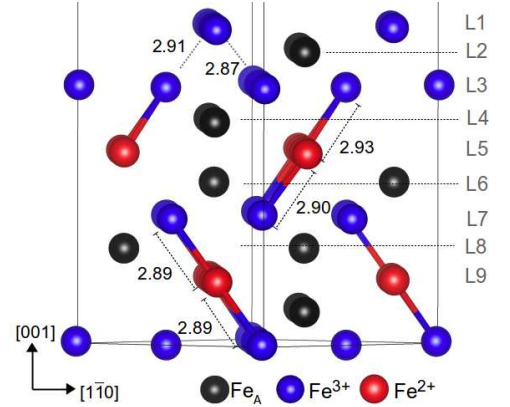


FIG. 7. (Color online) Side view of the Fe sublattice at the Fe^{2+} -ended $\text{Fe}_3\text{O}_4(001)$ surface below T_V , indicating the bulk-like trimers and providing selected d^{FF} values (in Å).

The surface can be constructed exposing either Fe^{3+} or Fe^{2+} planes, which has implications for the continuity of bulk trimers close to the surface, as shown in figures 7 and 9. The most stable situation by ~ 70 meV/f.u. corresponds to the Fe^{2+} -ended case in figure 7, that at difference with the Fe^{3+} termination, preserves the bulk CO up to the subsurface. This energy difference is much larger than that between the $(\sqrt{2} \times \sqrt{2})R45^\circ$ and (1×1) surfaces at high temperatures, evidencing the high impact of the bulk CO on the surface properties. We have

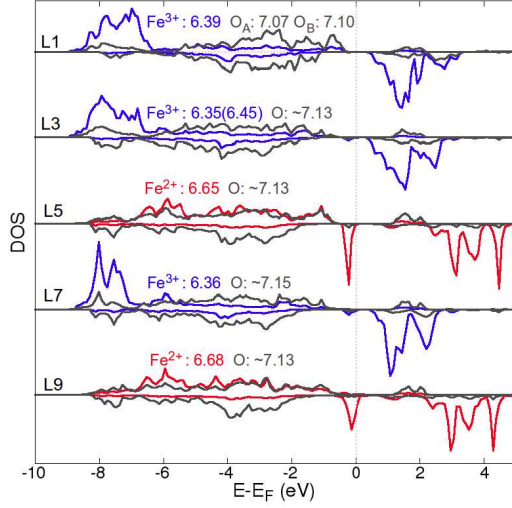


FIG. 8. (Color online) Layer- and spin-resolved DOS of the Fe^{3+} (blue), Fe^{2+} (red) and O (black) atoms of the structure in figure 7.

estimated that the loss of the bulk CO at the subsurface lowers the work function by 0.30 eV, a variation close to that induced by the adsorption of water³¹.

On the other hand, surface effects are similar to those at the HTP under both terminations: an insulating Fe^{3+} surface layer, shortened surface O- Fe_B bonds, and a similar pattern of outermost interlayer distances and longitudinal atomic displacements within the Fe_B rows. This helps to attain bulk values of the O charge, though the surface causes an additional dispersion in Q_B , as shown in figures 8 and 10 for the Fe^{2+} - and Fe^{3+} -ended cases, respectively. Surprisingly, at the Fe^{2+} termination the same electronic structure corresponds to the (1×1) and $(\sqrt{2} \times \sqrt{2})R45^\circ$ surfaces, separated by less than 7 meV/f.u. This is because the LTP bulk structure introduces an additional charge modulation within (001) planes, that obscures that induced by the reconstruction: regarding figure 7, half of the Fe^{3+} sites at L3 would develop trimerons with the upper Fe_B , but these have changed their valence inhibiting the polaronic charge distribution. As the other half participate in trimerons with the layers below, two types of Fe_B sites exist at the subsurface, with similar DOS but slightly different Q_B and interatomic distances to the surface Fe_B . Again this proves the influence of the bulk CO on the surface properties below T_V .

In turn, the robust insulating surface layer, which seems to be a universal feature of magnetite even under metastable terminations^{17,18}, has an important local effect on the bulk CO. This better manifests at the Fe^{3+} termination in figures 9 and 10, where the lack of continuity of the trimerons at the subsurface allows for the emergence of localized bipolarons, indicating the possible coexistence of local surface and bulk COs. But fig-

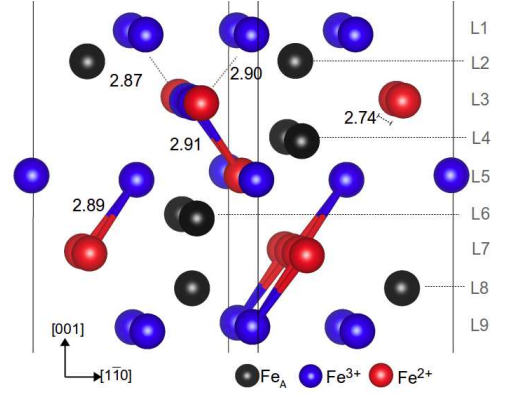


FIG. 9. (Color online) Same as figure 7 for the Fe^{3+} -ended surface of the LTP.

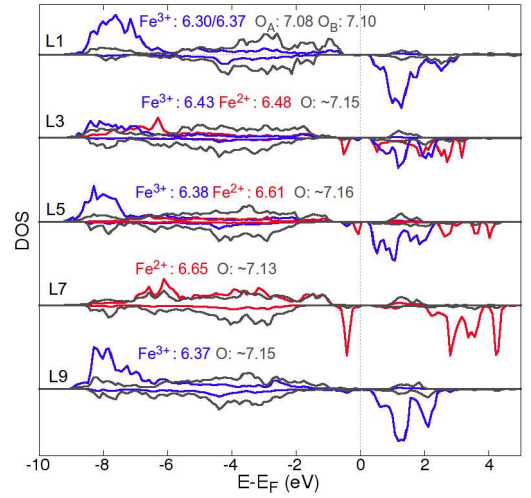


FIG. 10. (Color online) Same as figure 8 for the structure in figure 9.

ure 7 evidences that also at the Fe^{2+} termination those trimerons closer to the surface are slightly affected by it: the Fe^{3+} - Fe^{2+} distances between L3 and L5 are moderately enlarged, which introduces an asymmetry in the Fe chain weakening the charge sharing in its upper branch. In summary, though preservation of the bulk CO seems to have a dominant effect on the surface stability, it is conditioned by the insulating Fe^{3+} surface layer, and there is a mutual influence of the bulk and surface properties that extends several layers below the surface plane.

VI. SUMMARY AND CONCLUSIONS

Our results prove that the $\text{Fe}_3\text{O}_4(001)$ surface shows a robust insulating state that persists across the surface and bulk phase transitions. It is originated by the large demand of charge from surface O arising from

bond breaking, and causes a significant restructuration at the outermost planes that inhibits the formation of trimers. Below T_S , a surface CO distinct from that of the bulk LTP emerges. Its distinct nature manifests in a lower charge disproportionation as compared to the bulk LTP, and in the preferential bipolaronic CO within (001) planes. When the temperature is lowered below T_V , this surface CO competes with the dominant bulk one. This competition is conditioned by the insulating Fe^{3+} character of the surface, which weakens the trimeron structures.

Besides its intrinsic interest, the relation between CO and dimensionality has implications for the multifunctional properties of magnetite, since the emergence of ferroelectric polarization⁹, the orientation of the magnetic easy axis²⁴ or the catalytic activity^{32,33} are related to the existence of different Fe_B sites and the resulting charge distribution. Direct evidence from surface measurements is challenging, as most effects will manifest at the subsurface level. Additional complications emerge

from the existence of APB in real samples, and from differences in the relative orientation of the monoclinic and cubic crystal axes in single crystals and thin films. From the theoretical side, the inclusion of the full Cc symmetry, with additional modulations of the CO within (001) planes, may show an even richer scenario. However, our results unequivocally demonstrate the existence of a mutual influence of the surface and bulk COs, providing and partially quantifying the main features involved in it. We hope they will motivate further work in this fascinating subject.

ACKNOWLEDGMENTS

This work has been financed by the Spanish Ministry of Science under contracts MAT2009-14578-C03-03 and MAT2012-38045-C04-04. I.B. acknowledges financial support from the JAE program of the CSIC.

-
- * sgallego@icmm.csic.es
- ¹ A. Orozco, S.B. Ogale, Y.H. Li, P. Fournier, E. Li, H. Asano, V. Smolyaninova, R. L. Greene, R.P. Sharma, R. Ramesh, and T. T. Venkatesan. *Physical Review Letters* **83**, 1680 (1999).
 - ² H.C. Wu, O.N. Mryasov, M. Abid, K. Radican, and I.V. Shvets. *newblock Scientific reports*, **3**, 1830 (2013).
 - ³ M. Liu, J. Hoffman, J. Wang, J. Zhang, B. Nelson-Cheeseman, and A. Bhattacharya. *Scientific reports* **3**, 1876 (2013).
 - ⁴ E.J.W. Verwey. *Nature* **144**, 327 (1939).
 - ⁵ I. Leonov, A.N. Yaresko, V.N. Antonov, M.A. Korotin, and V.I. Anisimov. *Physical Review Letters* **93**, 146404 (2004).
 - ⁶ D.J. Huang *et al.* *Physical Review Letters* **96**, 096401 (2006).
 - ⁷ M. M. Iizumi, T.F. Koetzle, G. Shirane, S. Chikazumi, M. Matsui, and S. Todo. *Acta Crystallographica B* **38**, 2121 (1982).
 - ⁸ H.-T. Jeng, G.Y. Guo, and D.J. Huang. *Physical Review B* **74**, 195115 (2006).
 - ⁹ K. Yamauchi, T. Fukushima, and S. Picozzi. *Physical Review B* **79**, 212404 (2009).
 - ¹⁰ J. Blasco, J. García and G. Subías. *Physical Review B* **83**, 104105 (2011).
 - ¹¹ M.S. Senn, J.P. Wright, and J.P. Attfield. *Nature* **481**, 173 (2012).
 - ¹² F. Walz. *Journal of Physics: Condensed Matter* **14**, R285 (2002).
 - ¹³ J. García and G. Subías. *Journal of Physics: Condensed Matter* **16**, R145 (2004).
 - ¹⁴ M. Hoesch, P. Piekarz, A. Bosak, M. Le Tacon, M. Krisch, A. Kozłowski, A.M. Oleś, and K. Parlinski. *Physical Review Letters* **110**, 207204 (2013).
 - ¹⁵ A. Bosak, D. Chernyshov, M. Hoesch, P. Piekarz, M. Le Tacon, M. Krisch, A. Kozłowski, A.M. Oleś, and K. Parlinski. *Physical Review X* **4**, 011040 (2014).
 - ¹⁶ S. de Jong *et al.* *Nature materials* **12**, 882 (2013).
 - ¹⁷ K. Jordan, A. Cazacu, G. Manai, S.F. Ceballos, S. Murphy, and I.V. Shvets. *Physical Review B* **74**, 085416 (2006).
 - ¹⁸ Z. Lodziana. *Physical Review Letters* **99**, 206402 (2007).
 - ¹⁹ B. Stanka, W. Hebenstreit, U. Diebold, and S.A. Chambers. *Surface Science* **448**, 49 (2000).
 - ²⁰ I.V. Shvets, G. G. Mariotto, K. Jordan, N. Berdunov, R. Kantor, and S. Murphy. *Physical Review B* **70**, 155406 (2004).
 - ²¹ Z. Novotny, N. Mulakaluri, Z. Edes, M. Schmid, R. Pentcheva, U. Diebold, and G.S. Parkinson. *Physical Review B* **87**, 195410 (2013).
 - ²² R. Pentcheva, F. Wendler, H.L. Meyerheim, W. Moritz, N. Jedrecy, and M. Scheffler. *Physical Review Letters* **94**, 126101 (2005).
 - ²³ R. Pentcheva, W. Moritz, J. Rundgren, S. Frank, D. Schrupp, and M. Scheffler. *Surface Science* **602**, 1299 (2008).
 - ²⁴ J. de la Figuera, Z. Novotny, M. Setvin, T. Liu, Z. Mao, G. Chen, A.T. N'Diaye, M. Schmid, U. Diebold, A.K. Schmid, and G.S. Parkinson. *Physical Review B* **88**, 161410(R) (2013).
 - ²⁵ N.C. Bartelt, S. Nie, E. Starodub, I. Bernal-Villamil, S. Gallego, L. Vergara, K.F. McCarty, and J. de la Figuera. *Physical Review B* **88**, 235436 (2013).
 - ²⁶ G. Kresse and J. Hafner, *Physical Review B* **47**, 558 (1993); G. Kresse and J. Furthmüller, *Physical Review B* **54**, 11169 (1996).
 - ²⁷ P.E. Blochl, *Physical Review B* **50**, 17953 (1994); G. Kresse and J. Joubert, *Physical Review B* **59**, 1758 (1999).
 - ²⁸ S.L. Dudarev, G.A. Botton, S.Y. Savrasov, Humphreys C.J., and A.P. Sutton. *Physical Review B* **57**, 1505 (1998).
 - ²⁹ J.P. Wright, P.G. Radaelli, and J.P. Attfield. *Physical Review Letters* **87**, 266401 (2001); J.P. Wright, J.P. Attfield, and P.G. Radaelli. *Physical Review B* **66**, 214422 (2002).
 - ³⁰ G.S. Parkinson, T.A. Manz, Z. Novotny, P.T. Sprunger, R.L. Kurtz, M. Schmid, D.S. Sholl, and U. Diebold. *Physical Review B* **85**, 195450 (2012).
 - ³¹ T. Kendelewicz, S. Kaya, J.T. Newberg, H. Bluhm, N. Mulakaluri, W. Moritz, M. Scheffler, A. Nilsson, R. Pentcheva, and G.E. Brown Jr. *Journal of Physical Chemistry C* **117**, 2719 (2013).

- ³² F.N. Skomurski, S. Kerisit, and K.M. Rosso. *Geochimica and Cosmochimica Acta* **74**, 4234 (2010).
- ³³ G.S. Parkinson, Z. Novotny, G. Argentero, M. Schmid, J. Pavelec, R. Kosak, P. Blaha, and U. Diebold. *Nature materials* **12**, 724 (2013).